Introduction of the Magnetic Pulse Compressor (MPC) - Fundamental Review and Practical Application

Jaegu Choi†

Abstract - Magnetic switch is a kind of saturable inductor, which utilizes nonlinearity of the magnetization curve of ferromagnetic materials. The right understanding of the saturation phenomena, magnetic properties, voltage-time product, and switching characteristics of the magnetic switch is essential in designing the magnetic pulse compressor (MPC). In this paper, the historical background of research on the MPC, fundamental physical properties of the magnetic switches, and application fields of the MPC are presented. Further, an in-depth analysis of pulse compression in series and parallel MPCs is incorporated. As practical application examples, a series MPC used for water treatments and a parallel MPC used for pulsed electric field (PEF) inactivation of bacteria are cited.

Keywords: Magnetic pulse compressor (MPC), Saturable inductor, Permeability, Pulsed electric field (PEF) inactivation

1. Introduction

Pulsed power has its foundation on nuclear fusion research, and since the 1st Pulsed Power Conference held in 1976, it has been recognized as a subject of scientific study. In those days, research on huge pulsed power generators, which generated large power with a one-shot operation, was vigorously carried out. In general, its application research was aimed at military purposes centering around two powers, namely, the USA and the USSR. Thereafter, with the collapse of the Cold War, a practical atmosphere for the application of the pulsed power technology to industrial purposes emerged. In the case where the pulsed power technology is used for industrial applications, research has been focused on the development of pulsed power generators that are eligible for high rep-rate operations with long-term high efficiency and reliability.

High speed switching is necessary for pulsed power generation, and discharge switches are used, including spark gap switches and thyratrons. However, these switches have critical problems due to electrode deterioration, resulting in unstable switching and short lifetime. The actual lifetime limits of a spark gap, a thyratron, and a semiconductor are estimated to be about 10^9, 3×10^9 and 10^{12}, respectively. Consequently, industrial pulsed power generators, to which high rep-rate operations are essential, adopt all solid-state switched circuits consisting of semiconductor switches and magnetic switches.

A magnetic switch consists of an inductor with a ferromagnetic core. The switching operation is realized using the variation of inductance due to nonlinear permeability, which is attributed to the saturation characteristics of the ferromagnetic material. The first magnetic pulse compressor (MPC) was realized by Melville in 1951 [1] as a radar power supply with the following specifications: output voltage of 13 kV, pulse duration of 250 ns, and peak power of 150 kW. However, because of response velocity, loss of the contemporary magnetic materials, as well as the cost and size of the system, the MPC has gone unnoticed for a while by the progress in the technology of spark gap switches, thyratron, and semi-conductor switches.

The recent development of ferromagnetic materials [2], [3] and semiconductor switches [4]-[7] with excellent characteristics has allowed the high repetitive operation of magnetic switches (MS) with very low loss. Moreover, the development made it possible to use the repetitive pulsed power generated by MPC on practical industrial applications, such as laser excitation, nuclear particle acceleration, radar modulation, EUV light source, and biochemical decontamination [8]-[18] due to its high repetition rate, high stability, and long lifetime.

2. Fundamental Theory of MPC

One of the best advantages of MPC is its ability to generate a large power with a high rep-rate, which is impossible with semiconductor switches. In other words, MPC temporally compacts electric power, which is controllable by semiconductor elements using magnetic switches and C-L-C resonant circuits. In this section, the physical properties of the magnetic switches are discussed.

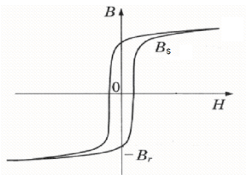

Fig. 1. Example of the magnetization curve of a ferromagnetic material.

† Corresponding Author: Pioneering Medical-Physics Research Center, KERI. (jgchoi@keri.re.kr)
Received: April 20, 2010; Accepted: June 15, 2010

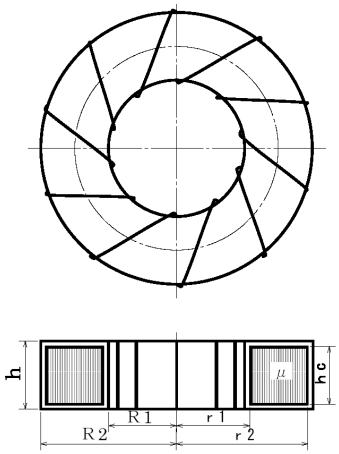

Fig. 2. Wound saturable inductor.

2.1 Principles of Magnetic Switches

Magnetic switch is a kind of saturable inductor, which utilizes the nonlinearity of the magnetization curve of ferromagnetic materials. The saturable switch is a variety of closing switch that performs the switching function using saturation phenomena, in which the unsaturation state of high inductance transfers to the saturation state of low inductance. Unsaturated inductance of a ring-shaped solenoid coil L_u [7] is represented by:

$$L_u = \frac{\mu_0 \mu_{ru} A N^2}{l}, \tag{1}$$

where μ_o and μ_{ru} are the free and unsaturated relative permeability, respectively, A is the magnetic material cross-section area, N is the number of conductor turns, and l is the magnetic field path length. On the other hand, saturated inductance L_s is represented by:

$$L_S = \frac{\mu_0 \mu_{rs} A N^2}{l}, \tag{2}$$

where μ_{rs} is the saturated relative permeability. The ratio of the unsaturated inductance to the saturated inductance L_u/L_s is given by (3).

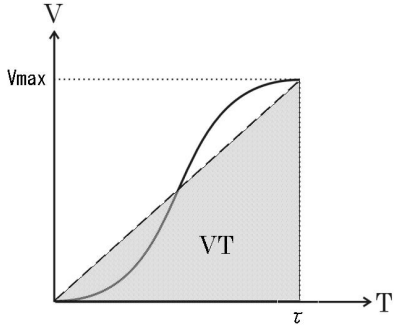

Fig. 3. Voltage-time product.

$$\frac{L_u}{L_s} = \frac{\mu_{ru}}{\mu_{rs}} \tag{3}$$

In general, the unsaturated relative permeability of ferromagnetic materials for saturable inductor μ_{ru} is several thousands to tens of thousands, and the saturated relative permeability μ_{rs} is about 1. Consequently, the switching function of the magnetic switch is realized by making use of this high inductance ratio.

2.2 Physical Properties of Magnetic Switches

As mentioned in the previous section, the performance of the magnetic switch is strongly dependent on the saturated and unsaturated permeability of the magnetic core. Main characteristics required of magnetic cores for the magnetic switch are as follows [19]:
(a) B_s is large;
(b) μ_{ru} is large and μ_{rs} is unity;
(c) Saturation occurs drastically;
(d) Loss is low; and
(e) Frequency dispersion is low.

An example of the magnetization curve of a magnetic material is shown in Fig.1. When a positive pulse voltage is applied to the saturable inductor, it is possible to obtain the maximum flux swing, $\triangle B_m$, as shown in (4) by biasing the magnetic material into reverse saturation as expressed by:

$$\Delta B_m = B_s - (-B_r), \tag{4}$$

where B_s is the saturation flux density.

2.3 Voltage-Time Product

The magnetic switch has no critical limitation for voltage and current in the similar manner that semiconductor switches have. However, the time at which the switch remains unsaturated is closely related with the applied voltage. The relationship between the voltage-time product and the flux density change [20] is expressed as:

$$\frac{1}{N}\int_0^{Ts} V(t)dt = \int_{Am} Bds = A_m \Delta B, \tag{5}$$

where T_s is time to saturation, V(t) is the applied voltage, $\triangle B$ is the magnetic flux density change or swing, and A_m is the magnetic material cross-section area.

A saturable inductor wound with coil is shown in Fig. 2. The actual magnetic core has SiO_2 films or polymer films, such as PET, for insulation between magnetic material layers. Stacking factor, K_{sf}, which is the ratio required by the magnetic material to occupy the magnetic core cross-section area $[A = hc(r_2 - r_1)]$, is represented by:

$$K_{sf} = \frac{A_m}{A}. \quad (6)$$

The minimum voltage-time product required for the saturation of a magnetic switch is described by (7) and Fig. 3 as follows:

$$\int_0^{\tau} V(t)dt = \frac{V_{\max}\tau}{2} = NA_m\Delta B. \quad (7)$$

From (7), it can be seen that the time to saturation of the saturable inductor is determined by the applied voltage, cross-section area, and number of winding turns.

2.4 Switching Characteristics

The magnetic switch is not an active switch just like a thyratron or a thyrister, but a passive switch that utilizes the magnetic saturation of the magnetic material. The applied voltage is maintained and the current is almost blocked by high inductance during core unsaturation, resulting in the off state of the magnetic switch. On the other hand, the current flows with the low inductance during core saturation, resulting in the on state. The inductance of the magnetic switch, shown in Fig. 2, is given by:

$$L \cong \mu \frac{N^2 h}{2\pi} \ln \frac{R_2}{R_1}, \quad (8)$$

where μ is the permeability of the magnetic material, h is the height of the cross-section area that the winding encloses, R_2 is the outer radius of the winding, and R_1 is the inner radius of the winding. If it is assumed that the saturated relative permeability μ_r is almost 1, the saturated inductance of the magnetic switch L_t is given by:

$$L_t \cong \mu_0 \frac{N^2 h}{2\pi} \ln \frac{R_2}{R_1}. \quad (9)$$

3. Application Fields of the MPC

Temporally and spatially compacted pulsed power, both of which have a relatively small energy and huge power, can be used for unprecedented application fields such as laser excitation, nuclear particle acceleration, radar modulation, biochemical decontamination, and so on.

The repetitive pulsed power can be used for the excitation of transversely excited atmospheric (TEA) CO_2 lasers and excimer lasers. TEA CO_2 laser is an infrared laser with a wavelength in the 9-11 μm range, has a highest radiation efficiency (>10%) among gas lasers. TEA CO_2 laser excited in medium gas pressure higher than 1 atm emits a laser light of very high Q. In particular, this laser can be used for laser marking and minute hole machining, thereby maximizing pulse characteristics. Semi-conductor switches and magnetic switches are adopted for the excitation circuit of the TEA CO_2 laser. The output of 3 kW is obtained with the rep-rate of 600 pps.

Excimer laser is a high power laser whose wavelength is in the ultraviolet range [21]. This is used for various laser processes, such as laser CVD, laser radar, ultra minute hole machining, TFT LCD annealing, cornea operation, and as EUV light source. Pulsed power supply is indispensable to both electron beam excitation and discharge excitation of the excimer laser. High voltage (tens of kV) with fast rise time (<200 ns) is applied to the discharge tube of the laser. The rep-rate is hundreds of pps.

Particle accelerator was first developed for the elementary particle experiments. At present, small-sized electron beam accelerators are being used for radiation treatments and the generation of radioactive lights [22].

Magnetron, whose drive circuit is a high rep-rate pulse power generator, is used for the radar transmitter (Radio Detection and Ranging). Melville reported a pulsed power supply, which adopted magnetic switches in lieu of thyratron switches, for a radar in 1951 [1].

Applications of the pulsed power discharge have been studied to reduce nitrogen oxides (NOx) and sulfur oxides (SOx) contained in the flue gases resulting from coal-burning power plants, factories, steel plants, and automobile exhausts [10]-[13]. In order to obtain the accelerated free electrons, a power supply for fast-rising narrow high-voltage pulses is necessary. The energetic electrons directly react on the harmful gas molecules or generate active radicals that dissociate the molecules.

As bio-related applications of pulsed power, sterilization, water treatment [23], and intracellular electromanipulation have been watched with keen interest. Sterilization using pulsed power is a very effective method to kill bacteria while avoiding thermal damages to the medium. The effects of pulsed power discharge in water on cyanobacteria cells have been investigated as well [24]. As a result, it has been found that the shockwave and discharge current brought about by the pulsed streamer-like discharge in water are the effective factors for the collapse of gas vesicles. Recently, studies on intracellular electromanipulation to verify the effect of short pulses on cells and tissue have been intensively carried out [25], [26]. With subnanosecond pulses, generating electric fields in the plasma membrane and any intracellular membrane in excess of 2 MV/cm that are large enough to cause changes in molecular structures has become possible.

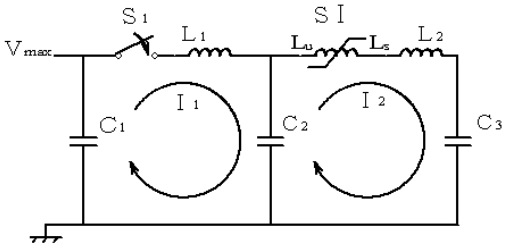

Fig. 4. Series MPC using a saturable inductor.

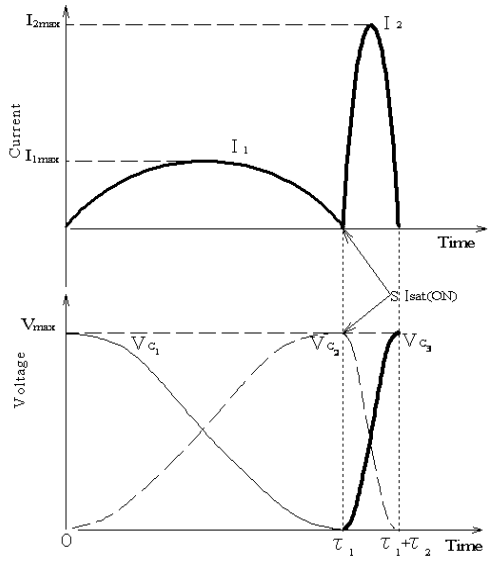

Fig. 5. Current and voltage waveforms of the series MPC.

4. Practical Application Examples

4.1 Series Magnetic Pulse Compressors

In this section, the operation mechanism of a series MPC [26]-[28] is addressed. Subsequently, an example of the series MPCs is presented. MPC uses a resonant energy transfer circuit shown in Fig. 4. L_1 is the stray inductance of the loop in which current I_1 flows, and L_2 is the stray inductance of the loop in which current I_2 flows. L_u and L_s are the unsaturated and saturated inductances of SI, respectively ($L_u \gg L_s$). It is supposed that $C_1 = C_2 = C_3$.

A power supply charges capacitor C_1 to voltage Vmax. The energy stored in capacitor C_1 is resonantly transferred to capacitor C_2 through inductor L_1 by closing switch S_1 at time t=0. Not until the energy is fully transferred from C_1 to C_2 that SI is saturated. At this moment, no energy is transferred from C_1 to C_3 because of high inductance L_u.

This circuit equation is given by:

$$V_{\max} = \frac{1}{C_1}\int I_1 dt + L_1 \frac{di}{dt} + \frac{1}{C_2}\int I_1 dt \cdot \tag{10}$$

The solution of (10) is given by:

$$I_1(t) = V_{\max}\sqrt{\frac{C_{12}}{L_1}}\sin\frac{t}{\sqrt{L_1 C_{12}}}, \tag{11}$$

where $C_{12} = C_1C_2/(C_1 + C_2)$.

C_1=C_2, the maximum of current I_1 is obtained from (11) by:

$$I_{1\max} = V_{\max}\sqrt{\frac{C_{12}}{L_1}} = V_{\max}\sqrt{\frac{C_1}{2L_1}} \cdot \tag{12}$$

Voltage on C_2 is given by:

$$V_{C2}(t) = \frac{1}{C_2}\int idt = V_{\max}\frac{C_1}{C_1 + C_2}\left(1 - \cos\frac{t}{\sqrt{L_1 C_{12}}}\right) \cdot \tag{13}$$

The maximum of V_{C2} is given by:

$$V_{C2\max} = V_{\max} \tag{14}$$

at the following time response to the pulse duration of current I_1:

$$t = \tau_1 = \pi\sqrt{L_1 C_{12}} \ . \tag{15}$$

In succession, energy transfer from C_2 to C_3 is considered. The energy stored in C_2 is fully transferred to C_3 with saturation of SI at t= τ_1 if $L_1 \gg L_s + L_2$. The maximum of current I_2 is given by:

$$I_{2\max} = V_{C2\max}\sqrt{\frac{C_{23}}{L_2 + L_s}} = V_{\max}\sqrt{\frac{C_1}{2(L_2 + L_s)}}, \tag{16}$$

where $C_{23} = C_2C_3/(C_2 + C_3)$=C/2. Time required for the energy transfer from C_2 to C_3 is given by:

$$\tau_2 = \pi\sqrt{(L_2 + L_s)C_{23}} = \pi\sqrt{\frac{(L_2 + L_s)C_1}{2}} \ . \tag{17}$$

This is equal to the pulse duration of current I_2. The maximum voltage on each capacitor is consistent.

$$V_{C3\max} = V_{C2\max} = V_{\max} \tag{18}$$

The conditions for pulse compression are $\tau_1 > \tau_2$ and

$$L_1 > L_2 + L_3 \ . \tag{19}$$

The pulse compression ratio is given by

$$G_1 = \frac{\tau_1}{\tau_2} = \sqrt{\frac{L_1}{L_2 + L_s}} \ . \tag{20}$$

The current and voltage waveforms during the above energy transfer are shown in Fig. 5. Current amplification can be achieved, whereas voltage amplification is not possible in the case of series magnetic pulse compression.

As an example of the series MPCs, the block diagram of a repetitive pulsed power system developed for water treatment is presented in Fig. 6 [26]. The system consists of the MPC unit, Blumlein-type pulse forming network (BPFN) unit, and load unit. The MPC unit is used as a charging generator for the BPFN.

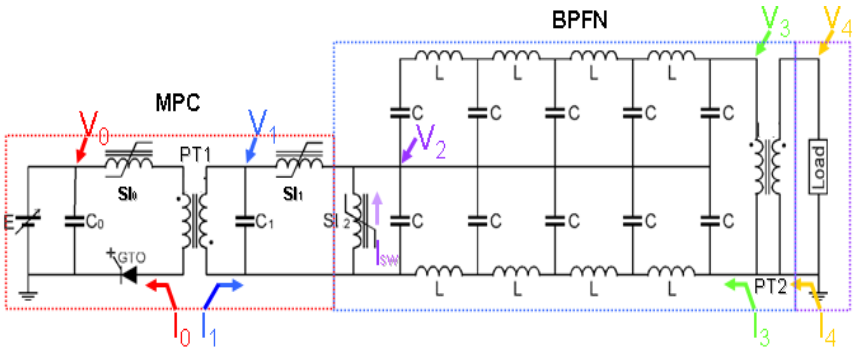

Fig. 6. Schematic diagram of the pulsed power generator for water treatments [4].

The MPC unit consists of a charger, low inductance capacitors (C0, C1), saturable inductors (SI0, SI1), a gate-turn-off thyristor (GTO), and a pulse transformer (PT1). The charger is a high voltage power supply, which uses resonant inverter (202 A, LAMBDA EMI). The average charging rate of the charger is 2000 J/s. The capacitances of C0 and C1 are 6.6 µF and 200 nF, respectively.

Fe-based nanocrystalline magnetic cores (FT-1H, Hitachi metals Ltd) were used as the magnetic switches (SI0, SI1). GTO is a high speed thyristor for pulsed power application (5STH20H4501, ABB). The shortcoming of spark gap switches, i.e., the deterioration of the gap, can be overcome by using this solid state switch. The magnetic assist by the saturable inductor (SI0) follows the GTO switching. Magnetic assist has the effect of reducing the switching loss of GTO [29]. Therefore, the MPC that consists of the magnetic switch and the solid state switch can be operated with higher repetition rate, longer lifetime, and higher reliability than conventional ones.

Fig. 7 shows the typical waveforms of the output voltage and current at the load unit, which consists of the point to plane electrode and the non-inductive resistor of 360 ohm in parallel. The output voltage V4 has 3 inherent peaks, namely, Peak 1, Peak 2, and Peak 3. Peak 1 is caused by the adoption of the reset circuit for the maximal flux swing of PT2. The peak appears until the core saturates in the negative direction. Peak 1 is undesirable, but unavoidable. Peak 2 originates from the non-uniform charging over the BPFN capacitors. Peak 3 is the main output voltage peak. The peak voltage, rise time, and pulse width at full wave half maximum (FWHM) are about 140 kV, 200 ns, and 1 µs respectively.

The developed pulsed power system in all solid state is shown in Fig. 8. The volume and the weight of the system are about 1 m^3 and 150 kg, respectively. A relatively large volume (≈34 cm^3) of streamer discharge was successfully generated in water with the developed system (Fig. 9). The streamer discharge grew radially from the tip of the positive point electrode. The propagation distance of the streamer was measured as about 35 mm with the naked eye. The streamer-like discharges generated by the developed system are being used for water treatments, such as sterilization of microorganisms and the decomposition of harmful materials.

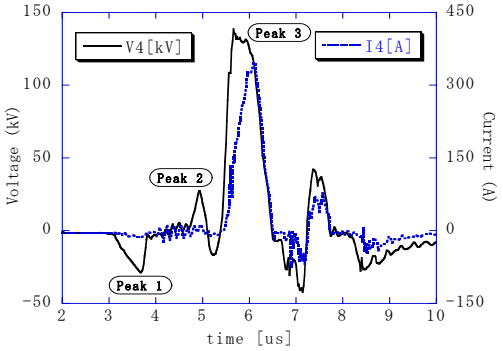

Fig. 7. Measured waveforms of V4 and I4 [4].

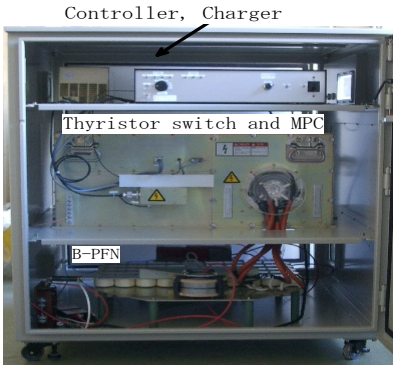

Fig. 8. Developed pulsed power system in a cube box [4].

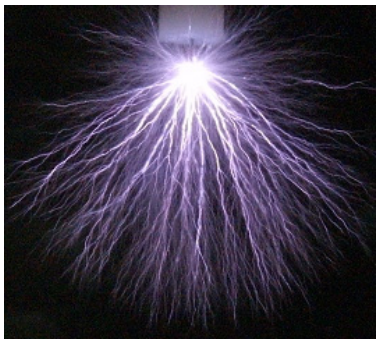

Fig. 9. Streamer-like discharge generated by the developed system in water. Electrode geometry**:** needle-to-plane. Radius of curvature at the needle tip: 30 µm. Electrode gap: 100 mm. Tap water conductivity: 25 mS/m [4].

4.2 Parallel Magnetic Pulse Compressors

Although a few reports [30], [31] have dealt with parallel magnetic pulse compressors, detailed explanations about the operation mechanism have not been provided. In this section, the operation mechanism of a parallel MPC is addressed using Figs. 10 and 11. Suppose that the turn ratio of ST is 1/n and $C_1 = n^2 \cdot C_2$, $C_2 = C_3$. Diode D is inserted in parallel with capacitor C3 in order to charge capacitor C2. L_1 is the stray inductance of the loop in which current I_1 flows, and L_2 is the stray inductance of the loop in which current I_2 flows. L_s is the saturated inductance of the secondary winding of ST.

A power supply charges capacitor C_1 to voltage Vmax. The energy stored in capacitor C_1 is resonantly transferred to capacitor C_2 through inductor L_1 and ST by closing switch S_1 at time t=0. It is not until the energy is fully transferred from C_1 to C_2 that ST is saturated. The maximum and the pulse duration of current I_1 are given by:

$$I_{1\ \max} = V_{\max} \sqrt{\frac{C_1}{2L_1}} \tag{21}$$

and

$$\tau_1 = \pi \sqrt{\frac{L_1 C_1}{2}} . \tag{22}$$

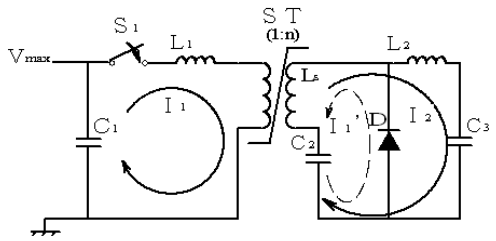

Fig. 10. Parallel MPC using a saturable transformer.

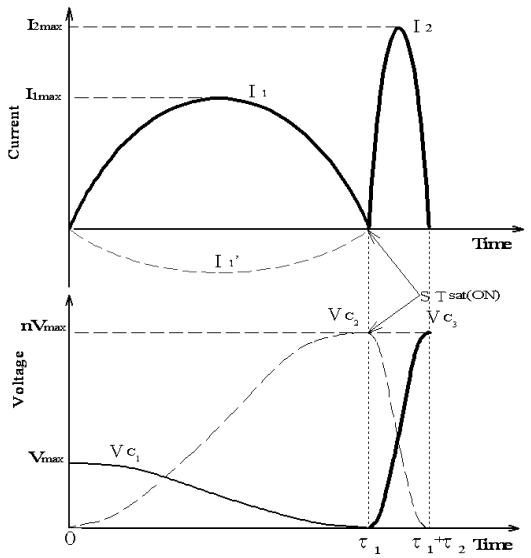

Fig. 11. Current and voltage waveforms of the parallel MPC.

The maximum voltage on C2 at time t= τ_1 , is given by:

$$V_{C2\ \max} = nV_{\max} . \tag{23}$$

Subsequently, energy transfer from C_2 to C_3 is considered. If ST is saturated at t= τ_1 , the transformer coupling breaks down, and the energy stored in C_2 is fully transferred to C_3. The maximum of current I_2 is given by:

$$I_{2\ \max} = V_{C2\ \max} \sqrt{\frac{C_2}{2(L_2 + L_s)}} . \tag{24}$$

The pulse duration of current I_2, which is the time required for the energy transfer from C_2 to C_3, is given by:

$$\tau_2 = \pi \sqrt{(L_2 + L_s) C_{23}} = \pi \sqrt{\frac{(L_2 + L_s) C_2}{2}} , \tag{25}$$

where $C_{23} = C_2 C_3/(C_2 + C_3) = C_2/2$. Given that C_1 is equal to $n^2 C_2$, the pulse compression ratio is given by:

$$G_{1ST} = \frac{\tau_1}{\tau_2} = \sqrt{\frac{L_1 C_1}{(L_2 + L_s) C_2}} = n \sqrt{\frac{L_1}{L_2 + L_s}} . \tag{26}$$

In principle, it is possible to obtain the same voltage gain as that of the turn ratio of ST in the case of parallel MPC. Consequently, a lower input voltage can be used for a pulse compression circuit, and the burden of a PT can be reduced with a lower turn ratio. The above discussion is limited only to ideal switches and transmission circuits. In actual circuits, losses in semiconductor switches, magnetic switches, and conductors should be considered.

On the other hand, pulsed electric field (PEF) inactivation is a very effective method to kill bacteria in liquid while avoiding thermal damage [32]. In this work, PEF with a maximum magnitude higher than 110 kV/cm and a pulse width of 100 ns was generated using a parallel MPC (Fig. 12). This was applied to a carefully designed treatment chamber through which a suspension fluid continuously flowed.

The pulsed power generator, which employs the parallel MPC, has a maximum output voltage of 60 kV, a pulse width at FWHM of 100 ns, and a repetition rate of 500 pps. Therefore, a maximum electric field of 150 kV/cm can be obtained using the treatment cell. The characteristic impedance is about 10 Ω [33]. Fig. 13 shows typical voltage and current waveforms at the treatment chamber in case of conductivity of 70 mS/m. It can be seen that the load is resistive from the phase of the waveforms. Consequently, the maximum electric field applied to the treatment chamber depends on the suspension conductivity. The instantaneous electrical power delivered to the load is 12 MW, but the average power is only about 100 W.

As a result, maximum 6.7 log reductions were achieved for *B. subtilis* using the proposed PEF inactivation method.

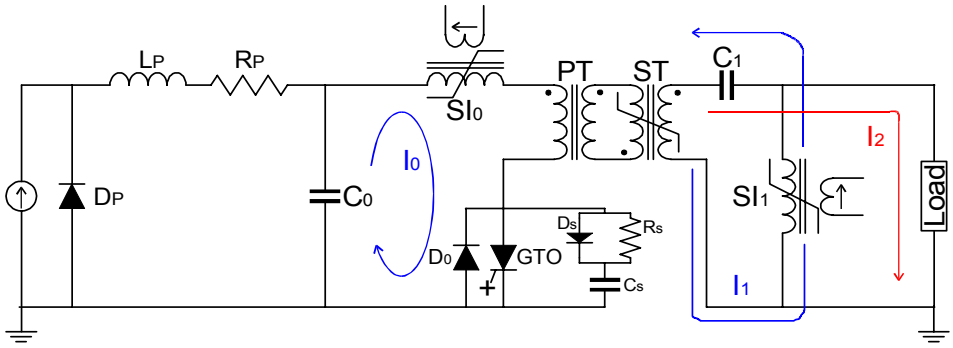

Fig. 12. Equivalent circuit diagram of the parallel MPC.

The transmission electron microscope (TEM) micrographs of *B. subtilis* spores showing the spore cross-section characteristics were obtained to verify the effect of the PEF treatment (Fig. 14). Upon exposure to heat (a conventional sterilization method), the color of the cortex slightly darkened and some deep dark spots in the core appeared, probably due to the leakage of some materials from the core. Upon exposure to PEF, the cortex grew much darker, and the deep dark spots in the core were observed clearly. These were caused by the irreversible loss of the function of the inner membrane.

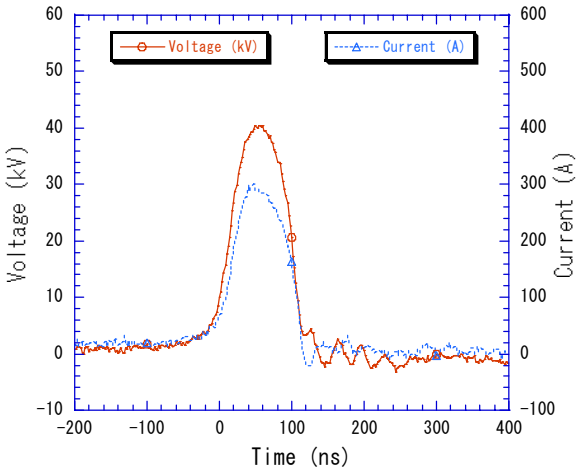

Fig. 13. Typical voltage and current waveforms (PEF: 100 kV/cm, conductivity: 70 mS/m) [10].

5. Conclusion

The historical background of the research on the MPC, fundamental physical properties of the magnetic switches, application fields of the MPC, and basic circuit theories of typical MPCs, as well as examples of practical application of the MPCs were presented with the aim of developing novel industrial applications of the MPC. In particular, two kinds of MPC that can be operated with high repetition rate, long lifetime, and high reliability for industrial applications were introduced. The output voltage of the series MPC showed a peak voltage, rise time, and pulse width (FWHM) of about 140 kV, 200 ns, and 1 μs, respectively. Water discharges were successfully generated with the developed system for practical industrial applications**.** PEF with a maximum magnitude higher than 110 kV/cm and a pulse width of 100 ns was generated by the parallel MPC, and were applied to a carefully designed treatment chamber through which a suspension fluid continuously flowed. Using the proposed PEF inactivation method, maximum 6.7 log reductions were achieved for *B. subtilis*.

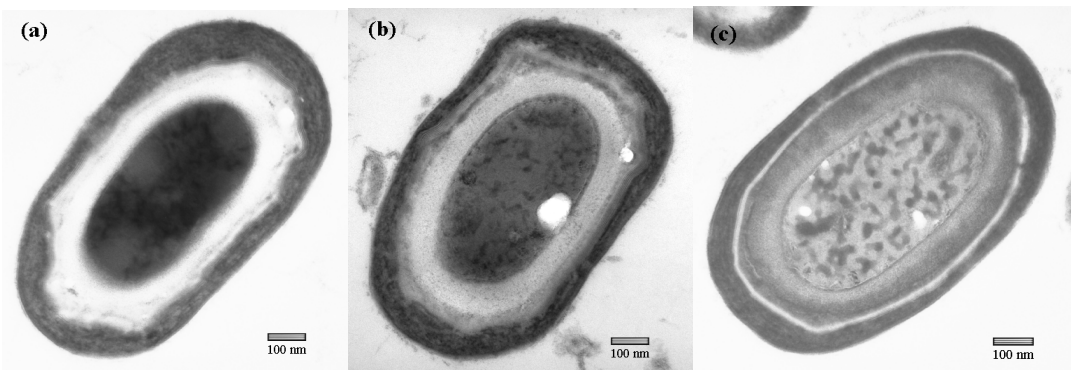

Fig. 14. TEM micrographs of *B. subtilis* spores showing the spore cross-section characteristics [10]. (a) control, (b) heat treatment (121 ℃), (c) PEF treatment. After exposure to heat and PEF, the cortex exposed to the latter grew darker and the deep dark spots in the core were observed more clearly, illustrating leakage of the core materials caused by the irreversible loss of the inner membrane's function.

TEM micrographs of *B. subtilis* spores verified the effect of the PEF treatment. The presented examples of the practical application are expected to contribute to the design of the nonlinear devices, develop novel industrial applications of the MPC, and broaden the application field of the MPC.

References

[1] W. S. Melville, "The Use of Saturable Inductors as Discharge Devices for Pulse Generators," *in Proceedings of Inst. Elec. Eng. Radio Section*. 98, pp.185-207, 1951.

[2] *Product Bulletin: Pulse Power Core, METGLAS*, Allied-Signal Inc., Parsippany, NJ, 1992.

[3] *FINEMET, Catalog No. HL-FM9-C*: Hitachi Metals, 2005.

[4] T. Sakugawa and H. Akiyama, "An all-solid-state pulsed-power generator using a high-speed gate-turn-off thyristor and a saturable transformer," *Electr. Eng. Japan*, Vol. 140, No. 4, pp.17-26, 2002.

[5] H. Rhinehart, R. Dougal and W. C. Nunnally, "Design and Analysis of a High Power 1kHz Magnetic Modulator," *in Proceedings of 5th IEEE Pulsed Power Conf.*, Arlington, VA, pp.660-663, 1985.

[6] P. W. Smith, *Transient Electronics Pulsed Circuit Technology*: John Wiley & Sons, Ltd., 2002.

[7] M. Hara and H. Akiyama, *High-voltage Pulsed Power Engineering*: Morikita Books, 1991 (In Japanese).

[8] W. Partlo, R. Sandstrom and I. Fomenkov, "A low cost of ownership KrF excimer laser using a novel pulse power and chamber configuration," *Intern. Soc. Optical Eng.-SPIE* , Vol. 2440, p.90, 1995.

[9] T. Shimada, M. Obara and A. Noguchi, "An All Solid-State Magnetic Switching Exciter for Pumping Excimer Lasers," *Rev. Sci. Instrum.*, Vol. 24, 44, 1985.

[10] T. Namihira, S. Tsukamoto, D. Wang, S. Katsuki, R. Hackam, H. Akiyama, Y. Uchida and M. Koike, "Improvement of NOx removal efficiency using short width pulsed power," *IEEE Trans. Plasma Sci*., Vol. 28, No. 2, pp.434-442, 2000.

[11] Y. Choi, H. Lee, G. Rim, T. Kim, G. Jang, W. Shin and Y. Song, "Analysis of the Pulsed Plasma Reactor Impedance for DeSOx and DeNOx," *Jpn. J. Appl. Phys*. Vol. 40, pp.1108-1113, 2001.

[12] Y. S. Mok, Ho W. Lee and Y. J. Hyun, "Flue gas treatment using pulsed corona discharge generated by magnetic pulse compression modulator," *J. Electrostatics* 53, pp.195-208, 2001.

[13] Y.-W. Choi, I.-W. Jeong, G.-H. Rim, E. P. Pavlov, C.-S. Choi, H.-K. Chang, M.-H. Woo and S.-P. LEE, "Development of a Magnetic Pulse Compression Modular for Flue Gas Treatment," *IEEE Trans. Plasma Sci*., Vol. 30, pp.1632-1636, 2002.

[14] G. Dinelli, L. Civitano and M. Rea, "Industrial Experiments on Pulse Corona Simultaneous Removal of NO_x and SO_2 from Flue Gas," *IEEE Trans. Indst. Appl*., Vol. 26, No. 3, pp.535-541, 1990.

[15] K. Watanabe, M. Mizuno, S. Nakajima, T. Iimura and Y. Miyai, "Development of a high performance core snubber for high power neutral beam injectors," *Rew. Sci. Ins*., Vol. 69, No. 12, pp.4136-4141, 1998.

[16] Z. He, J. Liu and W. Cai, "The important role of the hydroxy ion in phenol removal using pulsed corona discharge," *J. Electrostatics*, Vol. 63, (Is. 4), pp.371-386, 2005.

[17] E. Njatawidjaja, A. T. Sugiarto, T. Ohshima and M. Sato, "Decoloration of electrostatically atomized organic dye by the pulsed streamer corona discharge," *J. Electrostatics*, Vol. 63, (Is. 4), pp.353-359, 2005.

[18] W. Jiang, K. Yatsui, K. Takayama, M. Akemoto, E. Nakamura, N. Shimizu, A. Tokuchi, S. Rukin, V. Tarasenko and A. Panchenko, "Compact Solid-State Switched Pulsed Power and Its Applications," *in Proceedings of IEEE*, Vol. 92, pp.1180-1194, 2004.

[19] T. Sakugawa, "Development of a high-repetition-rate pulsed power generator and its applications" *Doctorate thesis*, Mar. 2004.

[20] T. Shimada, "Research on Magnetic Pulse Compressors for High Rep-rate Excimer Laser Excitation" *Doctorate thesis*, 1985.

[21] Nagai and Imazaki, "Pulsed Power Technology and Its Applications," *Journal of IEEJ*, Vol. 109, No. 6, p.453, 1989.

[22] T. Namihira, T. Yamaguchi, K. Yamamoto, Jaegu Choi, T. Kian, T. Sakugawa, S. Katsuki and H. Akiyama, "Characteristics of pulsed discharge plasma in water," *in Proceedings of IEEE Int. pulsed power conf*., pp.1013-1016, Monterey, CA. Jun. 2005.

[23] Z. Li, S. Sakai, C. Yamada, D. Wang, S. Chung, X. Lin, T. Namihira, S. Katsuki, and H. Akiyama, "The Effects of Pulsed Streamerlike Discharge on Cyanobacteria Cells," *IEEE Trans. Plasma Science*., Vol. 34, No. 5, pp.1719-11724, 2006.

[24] S.J. Beebe, P.M. Fox, L.J. Rec, K. Somers, R.H. Stark and K.H. Schoenbach "Nanosecond Pulsed Electric Field (nsPEF) Effects on Cells and Tissues: Apoptosis Induction and Tumor Growth Inhibition," *IEEE Trans. Plasma Science*, Vol. 30, No. 1, pp.286-292, 2002.

[25] Richard Nuccitelli, Uwe Pliquett, Xinhua Chen, Wentia Ford, R. James Swanson, Stephen J. Beebe, Juergen F. Kolb and Karl H. Schoenbach, "Nanosecond Pulsed electric fields cause melanomas to self-destruct," *Biochemical and Biophysical Research Communications (BBRC)*, Vol. 343, p.351, 2006.

[26] J. Choi, T. Yamaguchi, K. Yamamoto, T. Namihira, T. Sakugawa, S. Katsuki and H. Akiyama, "Feasibility Studies of EMTP Simulation for the Design of the Pulsed Power Generator using MPC and BPFN for Water treatments," *IEEE Transactions on Plasma Science*, Vol. 34, No. 5, pp.1744-1750, 2006.

[27] J. Choi, T. Namihira, T. Sakugawa, S. Katsuki and H. Akiyama," Simulation of 3-Staged MPC Using Custom Characteristics of Magnetic Cores," *IEEE Trans. on Dielectrics and Electrical Insulations*, Vol. 14, No.

4, pp.1025-1032, 2007.
[28] J. Choi, T. Namihira, T. Sakugawa, S. Katsuki and H. Akiyama, "Loss Characteristics of a Magnetic Core for Pulsed Power Applications," *IEEE Transactions on Plasma Science*, Vol. 35, No. 6, pp.1791-1796, 2007.
[29] T. Sakugawa and H. Akiyama, "An all-solid-state pulsed-power generator using a high-speed gate-turn-off thyristor and a saturable transformer," *Electr. Eng. Japan*, Vol. 140, No. 4, pp.17-26, 2002.
[30] Y. Teramoto, D. Deguchi, S. Katsuki, T. Namihira, H. Akiyama, I. Lisitsyn, "All-Solid-State Trigger-Less Repetitive Pulsed power Generator Utilizing Semiconductor Opening Switch," *in Proceedings of 13th IEEE Inter. Pulsed Power Conference*, pp.540-543, 2001.
[31] K. Kurihara, S. Kobayashi, I. Satoh, K. Shibata, M. Shigata, K. Masugata, K. Yatsui, "Magnetic Compressor Using Saturable Transformer to Excimer Lasers," *Rev. Sci. Instrum*. Vol. 63, No. 4, 1992.
[32] J. Choi, D. Wang, T. Namihira, S. Katsuki, H. Akiyama, X. Lin, H. Sato, H. Seta, H. Matsubara and T. Saeki, "Inactivation of Spores Using Pulsed Electric Field (PEF) in a Pressurized Flow System," *Journal of Applied Physics*, 104, 094701, 2008.
[33] N. G. Vasov, V. A. Danilychev, Y. M. Popov and D. D. Khodkevich: *Soviet Phys. JETP Lett*. 12, p.329, 1970.

Jaegu Choi received his B.E. and M.E. degrees from Kyoungpook National University, Daegu, Korea, in 1994 and 1996, respectively. He received his Ph.D. degree from Kumamoto University, Kumamoto, Japan. He is currently a senior researcher with the Korea Electrotechnology Research Institute, Ansan, Korea. His research interests include pulsed power application, atmospheric pressure plasma, power apparatus diagnosis, and breast tomosynthesis system.